Remote Sensing of Environment 208 (2018) 109–119

Contents lists available at ScienceDirect

Remote Sensing of Environment

journal homepage: www.elsevier.com/locate/rse

High resolution topobathymetry using a Pleiades-1 triplet: Moorea Island in 3D

Antoine Collin[a,b,*], James L. Hench[c], Yves Pastol[d], Serge Planes[b,e], Lauric Thiault[b,e], Russell J. Schmitt[f], Sally J. Holbrook[f], Neil Davies[g,h], Matthias Troyer[i,j]

[a] Ecole Pratique des Hautes Etudes, PSL Research University, Centre National de la Recherche Scientifique (UMR 6554 LETG), Dinard, Brittany, France
[b] LABoratoire d'EXcellence CORAIL, Perpignan, France
[c] Nicholas School of the Environment, Duke University, Beaufort, NC, United States
[d] Service Hydrographique et Océanographique de la Marine, Brest, France
[e] Ecole Pratique des Hautes Etudes, PSL Research University, Centre National de la Recherche Scientifique (USR 3278 CRIOBE), Papetoai, Moorea, French Polynesia
[f] Department of Ecology, Evolution and Marine Biology, Marine Science Institute, University of California Santa Barbara, Santa Barbara, CA, United States
[g] Gump South Pacific Research Station, University of California, Moorea, French Polynesia
[h] Berkeley Institute for Data Science, University of California, Berkeley, CA, United States
[i] Theoretische Physik, ETH Zurich, Zurich, Switzerland
[j] Microsoft Research, Redmond, WA, United States

ARTICLE INFO

Keywords:
Topobathymetry
Satellite
Optical
Photogrammetry
Light/water interactions
LiDAR

ABSTRACT

Worldwide the coastal land-sea interface is increasingly subject to natural and anthropogenic hazards. Monitoring this crucial interface may be addressed with satellite imagery as a cost-efficient mapping solution. Topography and bathymetry, defining the structural complexity of the coast, are commonly studied separately given specific thematic and methodological contexts, yet many science questions and societal challenges require an integrated approach (e.g., coastal inundation). In such cases, triplet multispectral imagery represents an affordable solution based on a single satellite product. Here we examine how Pleiades-1 triplet imagery may be used to retrieve a seamless and accurate topobathymetry digital surface model (DSM, from −20 to 1207 m) over an entire, socio-ecologically complex island: Moorea, French Polynesia. Creation of the topography DSMs was based on stereo and tri-stereo photogrammetry, and the bathymetry DSMs relied on quasi-nadiral multispectral data subject to light/water interaction modelling. Results were compared with over 3.9 million airborne LiDAR topobathymetry measurements to quantify how the spatio-spectral mode, the third imagery, and the level of radiometric correction act on two- and three-dimensional accuracy. Horizontal accuracy of the tri-stereo panchromatic dataset (E_{RMSE} = 4.22 and N_{RMSE} = 7.59 m) was better than the multispectral (E_{RMSE} = 5.06 and N_{RMSE} = 7.51 m) dataset. Topography point cloud density increased by a factor of three in the tri-stereo panchromatic (9.11 points/m^2) or multispectral (0.23 points/m^2) datasets. Topography vertical accuracy enhanced with tri-stereo + level-1 radiometric correction (RMSE = 7.40 m) for panchromatic and with stereo + level-1/-2 radiometric correction (RMSE = 7.77/7.77 m) as well as tri-stereo without radiometric correction (RMSE = 7.85 m) for multispectral datasets. Bathymetry vertical accuracy improved with level-2 (atmospheric) correction (RMSE = 0.83 m). Topobathymetry DSM derived from this optimized method has a wide spectrum of applications along coastal margins.

1. Introduction

The littoral zone is spatially complex, and high resolution topography and bathymetry are required to address many current global societal issues (Gesch et al., 2016). Seamless (land/sea) digital elevation models (DEM) based on novel data sources and processing have enabled coastal (emerged and benthic) habitat mapping (Collin et al., 2012; Collin et al., 2013), geomorphic process and sea-level height monitoring (Johnstone et al., 2016; Pe'eri et al., 2016), as well as risk delineation (Kress et al., 2016). Integrated approaches avoid the traditional divergence between terrestrial and marine scientists and stakeholder groups that have evolved with their own specific vertical datum, technologies, and approaches. At the global scale, topography has been derived from spaceborne data, such as the initial 90-m

* Corresponding author at: Ecole Pratique des Hautes Etudes, PSL Research University, Centre National de la Recherche Scientifique (UMR 6554 LETG), Dinard, Brittany, France.
E-mail address: antoine.collin@ephe.sorbonne.fr (A. Collin).

https://doi.org/10.1016/j.rse.2018.02.015
Received 11 August 2017; Received in revised form 8 January 2018; Accepted 12 February 2018
0034-4257/ © 2018 Elsevier Inc. All rights reserved.

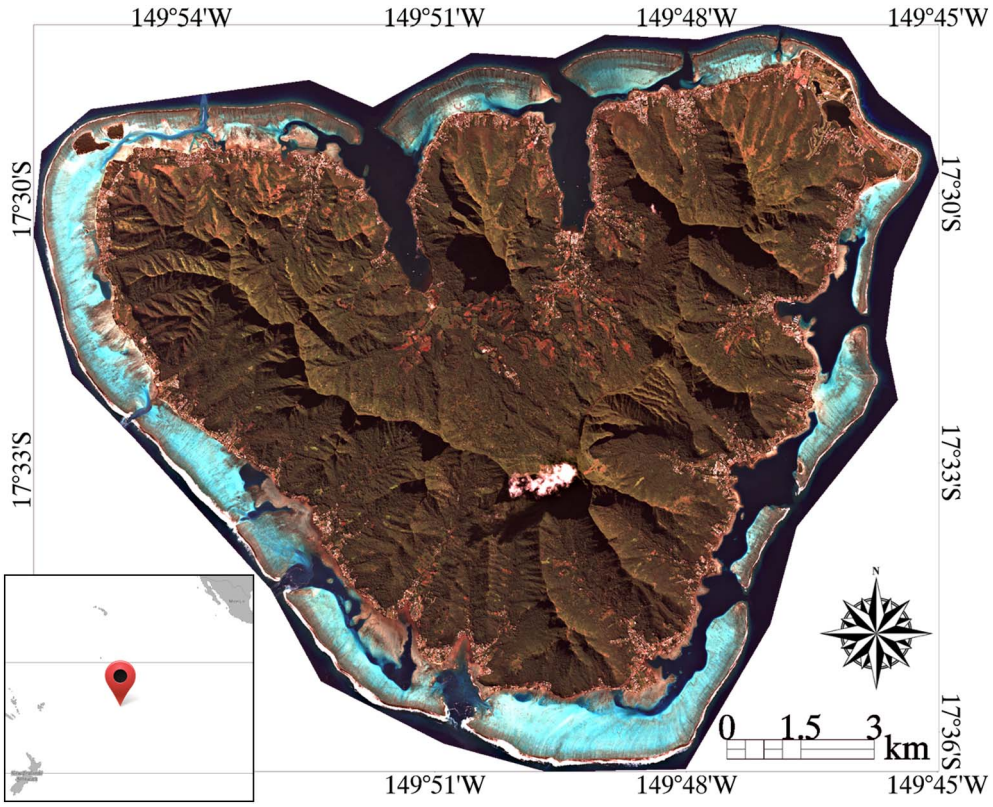

Fig. 1. Natural-colored imagery derived from the geometrically- and radiometrically-corrected blue, green and red Pleiades-1 wavebands collected over Moorea Island on June 23, 2014 (9193 × 7585 pixels). (For interpretation of the references to color in this figure legend, the reader is referred to the web version of this article.)

resolution shuttle radio detection and ranging (RaDAR) topography mission (SRTM, Farr et al., 2007), the 30-m advanced spaceborne thermal emission and reflection (ASTER) radiometer (Hayakawa et al., 2008), and the 12-m twin TerraSAR-X and TanDEM-X (Riegler et al., 2015). Worldwide bathymetry has been retrieved from inversion of the spaceborne 12-km geoid data (Geosat and European remote sensing satellite, ERS-1, Sandwell and Smith, 1997), and a combination of waterborne sound navigation and ranging (SoNAR) multibeam soundings from major marine agencies along with an improved gravity model from CryoSat-2 and Jason-1 with 500-m resolution (Olson et al., 2014). A 900-m resolution compilation of all available topography (SRTM, ASTER, spaceborne LiDAR for ice topography using ICESat and CryoSat-2) and bathymetry data (SoNAR, CryoSat-2 and Jason-1) has also been assembled (Becker et al., 2009).

Higher resolution (HR, 0.3–4 m range) topographic and bathymetric products conventionally rely on separated airborne and waterborne surveys, based on passive optical photogrammetry (Fonstad et al., 2013; Casella et al., 2016) or active SoNAR (Hayes and Gough, 2009). Airborne LiDAR using infrared and green wavelengths has played a key role in providing a continuous view of the littoral zone by simultaneously collecting HR data over land and water areas (Guenther et al., 2000). However airborne surveys need month-scale planning, calm sea, clement weather, and multi-thousand €/$ budgets. As an easier and cheaper alternative per unit area, HR multispectral spaceborne sensors have been used extensively for generating DEM or digital surface models (DSM) by applying the stereo-photogrammetric approach to pairs of IKONOS-2 (for soil DEM, Toutin, 2004a), Quickbird (for lake DEM, Toutin, 2004b), WorldView-1 or GeoEye-1 (for urban DSM, Capaldo et al., 2012) imageries. Urban and rural products from the tri-stereo Pleiades-1 (P-1) triplet have outperformed WorldView-2 and GeoEye-1 stereo-pairs (Poli et al., 2013). However, to our knowledge stereo and tri-stereo products have only been applied to land or water surface realms. In contrast, data from HR sensors have been used to extract digital depth models (DDM) by applying an empirical approach to single imagery: IKONOS-2 (Stumpf et al., 2003), QuickBird (Collin et al., 2014), WorldView-2 (Collin and Hench, 2012), P-1 (Collin and Hench, 2015), WorldView-3 (Collin et al., 2017).

Herein, we develop the first HR topobathymetry DSM (TBDSM) mostly based on an affordable spaceborne multispectral dataset, without need for specific fieldwork. We used 2-m resolution P-1 triplet imagery, constituted of blue, green, red, and infrared spectral data as the source data and created an optimized procedure accounting for spatial accuracy, spectral information and level of radiometric correction. Since 3D reconstruction based on satellite imagery relies on the pairwise search for corresponding pixels, provided with spectral values, in different imagery, we wish to test the influence of the radiometric correction, modifying spectral values. We appraise this approach on Moorea in French Polynesia, with the willing to transfer the method to a wide range of coastal areas. Encompassing the entire tropical island from 'ridge to reef', our study site spans structurally-complex terrestrial (mountain, forest, rural and urban areas) and benthic (mangrove, coral reef, macroalgae, sediment) systems. An infrared-driven mask was used to split land and sea areas to generate a land DSM from stereo and tri-stereo digital numbers (DN), top-of-atmosphere (TOA, i.e., at-sensor reflectance) and down-of-atmosphere (DOA, i.e., surface reflectance) reflectances, as well as create DDM from quasi-nadiral DN, TOA and DOA reflectances, and finally merge best land and sea models into a TBDSM (−20 to 1207 m). Comparisons with over 3.9 million measured values from an airborne LiDAR survey were used to quantify how the spatio-spectral mode, the third imagery and the level of radiometric correction act on two- and three-dimensional accuracy for both land and sea realms.

2. Materials and methods

2.1. Study site

The study site covers tropical volcanic island of Moorea (17° 29′ S, 149° 50′ W) located in the Society Archipelago in French Polynesia (Fig. 1). Formed some 1.6 million years ago, Moorea is a short distance from Tahiti. It rises 1207 m above sea level (Mount Tohiea) and lies on the Pacific oceanic crust, 4000-m below the waves. Covering 187 km^2 inside the barrier reef (134 km^2 land and 53 km^2 lagoon), Moorea features a wide variety of ecological habitats (cloud forest, native and invasive tree species, mangrove, coral reef, macroalgae, sediment), agriculture types (forestry, pineapple crop, pasture, aquaculture) and built areas (residential, agricultural and industrial, piers, roads, bridges), with nearly 17,000 inhabitants (2012 census). The heart-shaped island has two large bays on its north shore, one northeastern mangrove and saltmarsh, and a well-structured lagoon with fringing, barrier and outer reefs. Hosting two international research stations, the island is one of the most intensively studied in the world (Cressey, 2015).

2.2. Validation LiDAR dataset

An airborne topobathymetric LiDAR survey was carried out from June 10 to 26, 2015 using a Fugro LADS Mk 3 airborne system integrated with a RIEGL VQ-820-G hydrographic airborne laser scanner. The first sensor collected 5 m × 5 m laser spot spacing and the second sensor was operated at 251 kHz, providing a nominal sounding density of 4 points per m^2. Both sensors had a vertical accuracy (root mean square error, RMSE) of 0.4 m. The maximum depth obtained was 76.1 m, however the LiDAR dataset was cropped from −20 m to 300 m for comparison with the passive remotely-sensed P-1 data, whose accurate depth retrieval is limited by 20 m (Collin et al., 2014). For the sake of method transferability, original altimetric (*NGPF*) and geodetic (*RGPF*) systems were modified to global references (SHOM, 2016). The LiDAR altimetric system was referenced to the mean sea level (MSL) at Papetoai dock on the north shore of Moorea (SHOM, 2017). The geodetic system was resampled to WGS-84 and projected into the UTM 6 South coordinate system (Fig. 2). The LiDAR survey horizontal accuracy was quantified using an array of 67 ground control points identifiable over imagery (GCPs, red dots in Fig. 2), while 100 hydrographic soundings (blue dots in Fig. 2) were drawn from the digitalized *SHOM* navigational chart (#6657, based on 1966-to-1972 survey initially referenced to the lowest astronomical tide, namely hydrographic zero), then referenced to the MSL to calibrate the DDM. Despite the relatively long period separating SoNAR and LiDAR surveys, we assume that bathymetry did not vary considerably due to the century scale growth of corals. Topographic and bathymetric LiDAR soundings were rasterized (using regularly-gridded interpolation of Delaunay triangulation) at 2 m spatial resolution to quantify, on a common spatial scale, the vertical accuracy of tested TBDSMs (1,511,273 and 2,417,704 pixels, respectively).

2.3. Spaceborne triplet imagery

Spaceborne multispectral triplet imagery was acquired with the P-1 sensor on June 23, 2014 at 20 h 24 min 28 s UTC during 38 s over Moorea (Fig. 3 and Table 1). Water level at the nearest tidal reference station at Papeete was 0.03 m below MSL. Launched in 2011, P-1 records traditional one panchromatic and four optical bands at 0.7 m and 2.8 m pixel size (at nadir), and provides resampled imagery at 0.5 and 2 m, respectively. The scene coverage can reach 100 km × 100 km in a tri-stereo mode and the radiometric resolution per band is 12 bits. The panchromatic window ranges from 470 to 830 nm, and multispectral windows encompass blue (430–550 nm), green (500–620 nm), red (590–710 nm) and near-infrared (740–940 nm) wavebands. Sole satellite imagery orientation (defined by the rational polynomial coefficients, RPCs) was used to retrieve the topobathymetry without need for GCPs calibration. This choice is motivated to promote the transferability of the method where ground-truthing is difficult for logistic reasons. Consistent with the airborne LiDAR validation data, the WGS84 datum and the conformal, cylindrical UTM Zone 6 South projection was applied to the P-1 data. Panchromatic and multispectral datasets were radiometrically-corrected at the first level by standardizing the solar irradiance and calibrating the 12-bit DN into TOA reflectance, then at the second level, by compensating for the atmosphere interactions with P-1 wavebands (using the MODTRAN4-based algorithm), thus computing DOA reflectance (see Collin and Hench, 2012 for details). A threshold value based on the near-infrared information was used for discriminating (masking out) land and sea areas that will be subject to subsequent topography and bathymetry specific processing.

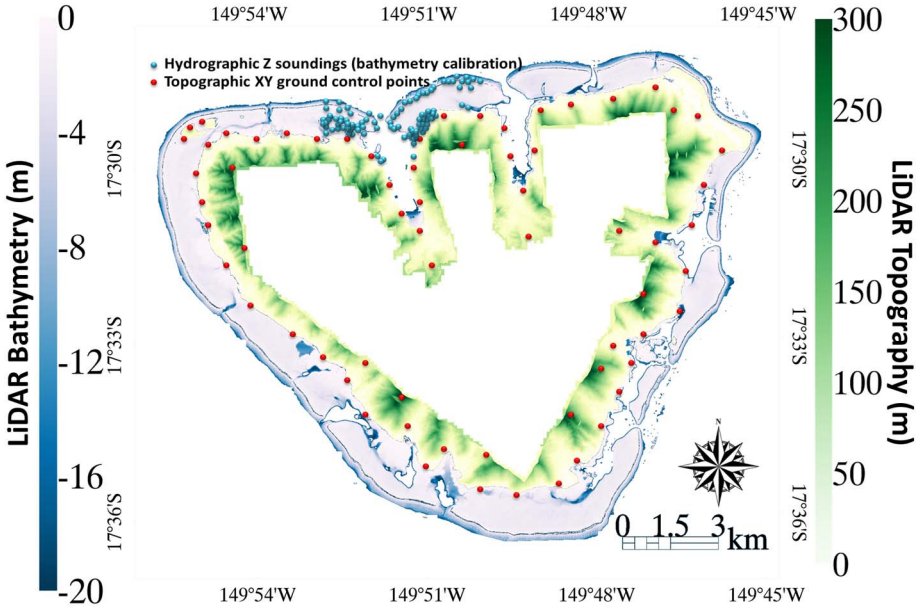

Fig. 2. Topobathymetry digital surface model (m) of Moorea coastal fringe derived from a combination of LiDAR infrared-based topographic survey (green color ramp based on the MSL) and LiDAR green-based hydrographic survey (blue color ramp based on the MSL). Red points represent locations of the topographic ground control points, while blue points represent locations of the hydrographic soundings derived from *SHOM* navigational chart. (For interpretation of the references to color in this figure legend, the reader is referred to the web version of this article.)

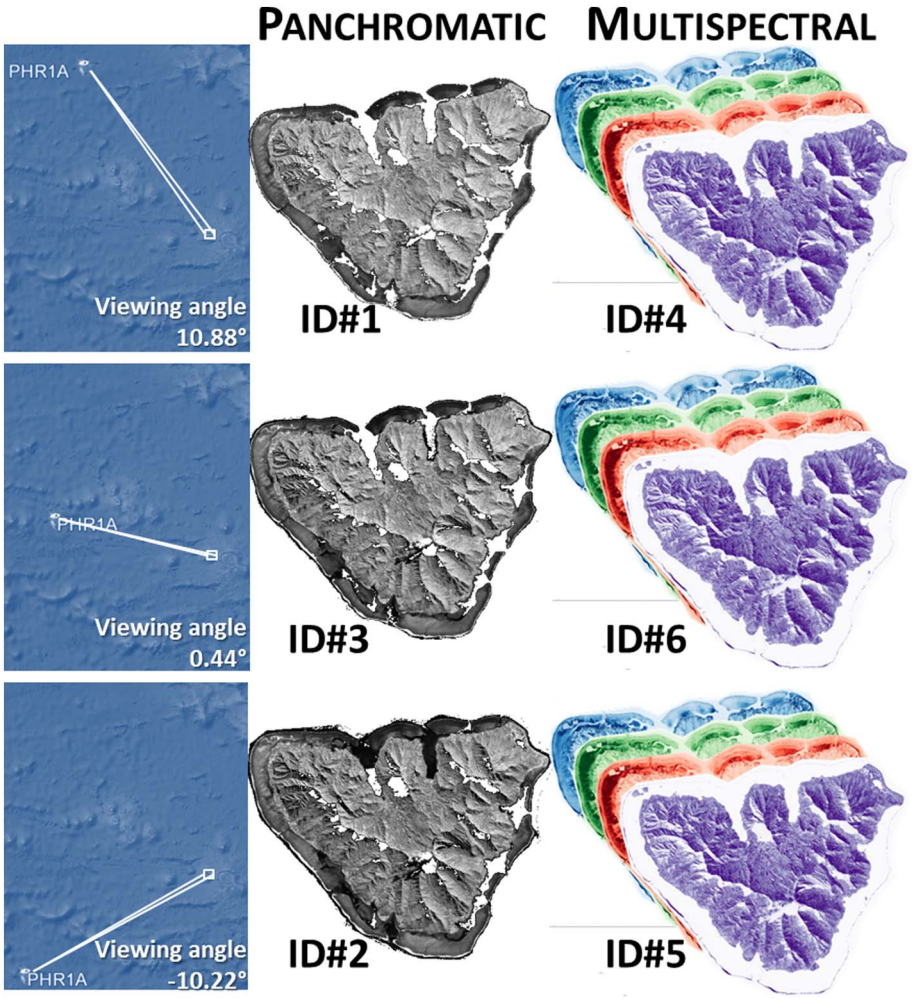

Fig. 3. Spectral datasets of the triplet Pleiades-1 imagery, each containing four 2-m multispectral and one 0.5-m panchromatic wavebands, for three viewing angles.

Table 1
Acquisition specificities related to the Pleiades-1 triplet imagery.

		Imagery #1#4	Imagery #3#6	Imagery #2#5
Date		2014-06-23	2014-06-23	2014-06-23
Time		20:24:28	20:24:47	20:25:06
Orientation angle (°)		180.02	180.04	180.03
Incidence angle	Across track	−8.43	−10.79	−13.18
(°)	Along track	−13.55	−2.18	9.55
Viewing angle	Across track	9.18	9.86	10.51
(°)	Along track	10.88	0.44	−10.22
Sun angle (°)	Azimuth	31.07	31.07	30.80
	Elevation	42.70	42.70	42.82

2.4. Topography processing

Once land areas were masked, a comparison workflow was established to examine the influence of the spatio-spectral mode, the third imagery, and the level of radiometric correction on topographic accuracy. Two panchromatic (DN and TOA) and three multispectral (DN, TOA and DOA) datasets, each composed of a triplet imagery, were used for 3D point cloud generation from the semi-global matching algorithm (Gehrke et al., 2010), DSM creation, and LiDAR comparison (Fig. 4A). The matching algorithm optimizes the pairwise search for corresponding pixels of two images by reducing the epipolar 2D dimensions to 1D, based on RPCs, then by shortening the length of the epipolar line with a 30-arcsecond global multi-resolution terrain elevation data (GMTED) 2010 dataset (Danielson and Gesch, 2011). Point clouds altitude were referenced to MSL, and DSMs were created at 2 m spatial resolution (equal to imagery resolution) to test the highest resolution, even if a DSM computed with twice the pixel size of original imagery is safer to increase the signal-to-noise ratio. The ENVI Photogrammetry and LiDAR modules were used to generate point clouds and create DSMs, respectively (Harris geospatial solutions, Broomfield, CO, USA, 2017).

2.5. Bathymetry processing

Sea areas were investigated to quantify the contribution of the level of radiometric correction applied to the quasi-nadiral (along-track viewing angle: 0.44°) multispectral imagery on bathymetric accuracy. Three multispectral (DN, TOA and DOA) datasets were subjected to ratio transform (Stumpf et al., 2003), DSM creation at 2-m spatial resolution, and LiDAR comparison (Fig. 4B). Based on the assumption that light decaying in water varies with wavebands, ratio transform elucidates the bathymetry (z):

$$z = a_1 \left(\frac{\ln[R_w(\lambda_i) - R_\infty(\lambda_i)]}{\ln[R_w(\lambda_j) - R_\infty(\lambda_j)]} \right) - a_0 \quad (1)$$

where a_0 is the offset to the MSL, a_1 is the slope scaling the relative to actual bathymetry (100 blue dots in Fig. 2), R_w is the DN/TOA/DOA reflectance related to the waveband λ_i, and R_∞ is the DN/TOA/DOA reflectance above optically deep water.

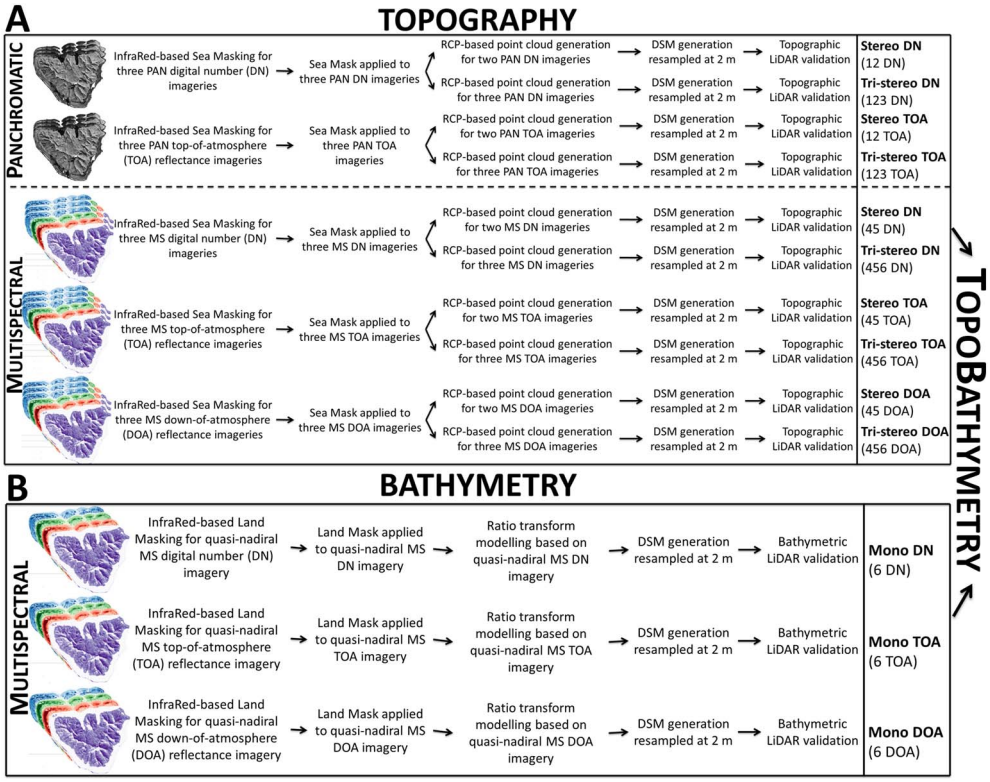

Fig. 4. Heuristic flowchart for the accuracy comparisons of both (A) topography and (B) bathymetry products derived from triplet Pleiades-1 imagery so as to merge best products into the topobathymetry digital surface model.

2.6. Accuracy analysis

The geolocation (horizontal) and height/depth (vertical) accuracies of P-1 modeled topobathymetry were quantified by comparison with 67 easting-northing GCPs and 3,928,977 LiDAR validation pixels. The horizontal and vertical accuracies were determined using mean and associated RMSE of both datasets' difference.

3. Results

3.1. Geolocation accuracy

The contribution of the third imagery to the geolocation (easting, *E*, and northing, *N*) accuracy of topography DSMs was evaluated for two spatio-spectral modes and three levels of radiometric corrections (Table 2). The addition of the third imagery to the conventional stereo models consistently increased the accuracy of both easting and northing coordinates. The highest accuracies in easting and northing positioning were found with panchromatic (E_{RMSE} = 4.22 m) and multispectral (N_{RMSE} = 7.51 m) tri-stereo models. Geolocation accuracy of tri-stereo models decreased from DN to TOA for panchromatic models, then from DN, DOA and TOA for multispectral models.

3.2. Height accuracy

The influence of third imagery on the generation of topographic point density (number of points per m^2) was mapped at 2 m spatial resolution for two spatio-spectral modes and three levels of radiometric corrections (Fig. 5). Lattices of areas provided with higher point density revealed higher mean values for panchromatic (5.92 pts./m^2) versus multispectral modes (0.4 pt./m^2). Inclusion of the third imagery yielded a factor three more points, irrespective of the spectral mode (see color ramp ranges in Fig. 5). Level 0 radiometric correction (i.e., DN, 9.11 and 0.63 pts./m^2) showed highest point density for tri-stereo panchromatic and multispectral modes, followed by level 1 radiometric correction (i.e., TOA, 9.07 pts./m^2) for panchromatic mode, followed by level 2 (i.e., DOA, 0.6 pt./m^2), and finally level 1 (TOA, 0.5 pt./m^2) for multispectral mode.

Topography DSMs were rendered at 2 m spatial resolution as functions of spatio-spectral modes and radiometric corrections within the

Table 2
Geolocation accuracy (2D) of topography digital surface models generated for three levels of radiometric corrections (digital number, top-of-atmosphere and down-of-atmosphere) and two photogrammetric modes (stereo and tri-stereo) as a function of Pleiades-1 spectral datasets (panchromatic, PAN, and multispectral, MS). Accuracies are based on mean differences and root mean squared error (RMSE) values of 67 ground control points (identifiable over imagery) defined with Easting (E) and Northing (N).

		Digital number				Top-of-atmosphere				Down-of-atmosphere			
		Mean diff.		RMSE		Mean diff.		RMSE		Mean diff.		RMSE	
		E	N	E	N	E	N	E	N	E	N	E	N
PAN	Stereo	−0.08	−0.86	4.88	8.35	−0.04	−0.77	4.93	7.92				
	Tri-stereo	−0.02	−0.65	4.22	7.59	−0.06	−0.72	4.47	7.85				
MS	Stereo	−0.11	−0.46	5.72	7.75	−0.34	−0.32	6.61	7.83	0.09	−0.62	5.21	7.89
	Tri-stereo	−0.04	−0.10	5.06	7.51	0.06	−0.62	5.75	7.88	0.02	−0.32	5.13	7.67

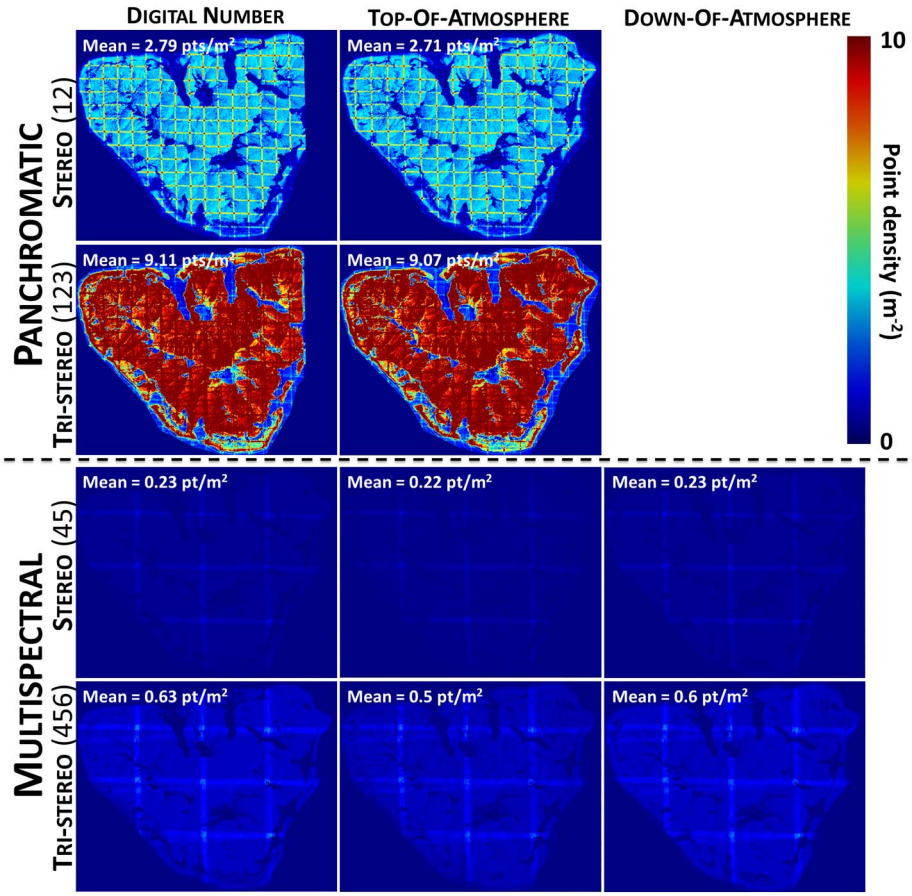

Fig. 5. Digital density models of the 3D topographic point clouds (point number per m^2) generated for three levels of radiometric corrections (digital number, top-of-atmosphere and down-of-atmosphere) and two photogrammetric modes (stereo and tri-stereo) as a function of Pleiades-1 spectral datasets (panchromatic and multispectral).

0–1207 height range (Fig. 6). Accuracies in height modelling were quantified by comparison with corresponding 0–300 m elevation range LiDAR topography DSM (Fig. 7). Highest accuracy was found with panchromatic tri-stereo mode with radiometric level 1 (TOA, RMSE = 7.40 m), while lowest accuracy resulted from panchromatic stereo mode of radiometric level 1 (RMSE = 8.31 m). Contrary to expectation from the underlying point density, panchromatic mode did not consistently show the best performance for height accuracy. DSMs derived from multispectral stereo TOA (RMSE = 7.77 m) and DOA (RMSE = 7.77 m) as well as tri-stereo DN (RMSE = 7.85 m) and TOA (RMSE = 8.04 m) were equal or more accurate than panchromatic stereo DN (RMSE = 8.01 m), TOA (RMSE = 8.31 m), and tri-stereo DN (RMSE = 8.18 m). Likewise, the addition of the third imagery into stereo datasets did not invariably improve height accuracy, as attested by panchromatic DN (RMSE = 8.01 to 8.18 m), multispectral TOA (RMSE = 7.77 to 8.04 m) and DOA (RMSE = 7.77 to 8.30 m). The examination of the radiometric correction on height accuracy indicated that converting DN to TOA benefited panchromatic tri-stereo (RMSE = 8.18 to 7.40 m) and multispectral stereo (RMSE = 8.15 to 7.77 m). TOA-to-DOA correction did not enhance accuracy for multispectral stereo (RMSE = 7.77 to 7.77 m) nor tri-stereo (RMSE = 8.04 to 8.30 m).

3.3. Depth accuracy

Bathymetry DSMs were built from the quasi-nadiral (mono) multispectral imagery using radiometric corrections within the 0–20 depth range (Fig. 8). Accuracies in depth predictions were estimated by comparison with 0–20 m range LiDAR bathymetry DSM (Fig. 9). The best agreement with the LiDAR data was produced with the level 2 of radiometric correction (DOA, RMSE = 0.83 m), followed by level 0 (RMSE = 1.06 m) and level 1 (RMSE = 1.17 m).

3.4. Topobathymetry modelling

A topobathymetry DSM was created by combining the most accurate topography and bathymetry DSMs, by means of the MSL reference. Topography, derived from the panchromatic tri-stereo imagery corrected at the TOA (radiometry level 1), was adjusted to the MSL by removing the intercept (i.e., 18.49 m, Fig. 10a). Bathymetry, derived from the multispectral quasi-nadiral (mono) imagery corrected at the DOA (radiometry level 2), was adjusted to the MSL by removing the offset (i.e., −0.47 m, Fig. 10b). Both were then merged into a seamless topobathymetry reef- and land-scape ranging from −20 to 1207 m (Fig. 10c).

4. Discussion

4.1. Drivers of the horizontal accuracy

The geolocation accuracy was influenced by the spatio-spectral mode, scene coverage and radiometry level. The increase in temporal resolution, identified by the addition of the third imagery (tri-stereo versus stereo), largely resulted in increased horizontal accuracy for both easting and northing positioning. The spatio-spectral mode, provided with initial finer spatial resolution but a single waveband (panchromatic), enabled better accuracy to be reached. Finally, the absence of radiometric correction consistently yielded the best accuracy. The most accurate coordinates' couple was achieved with higher initial spatial resolution, a single large waveband, higher coverage, and

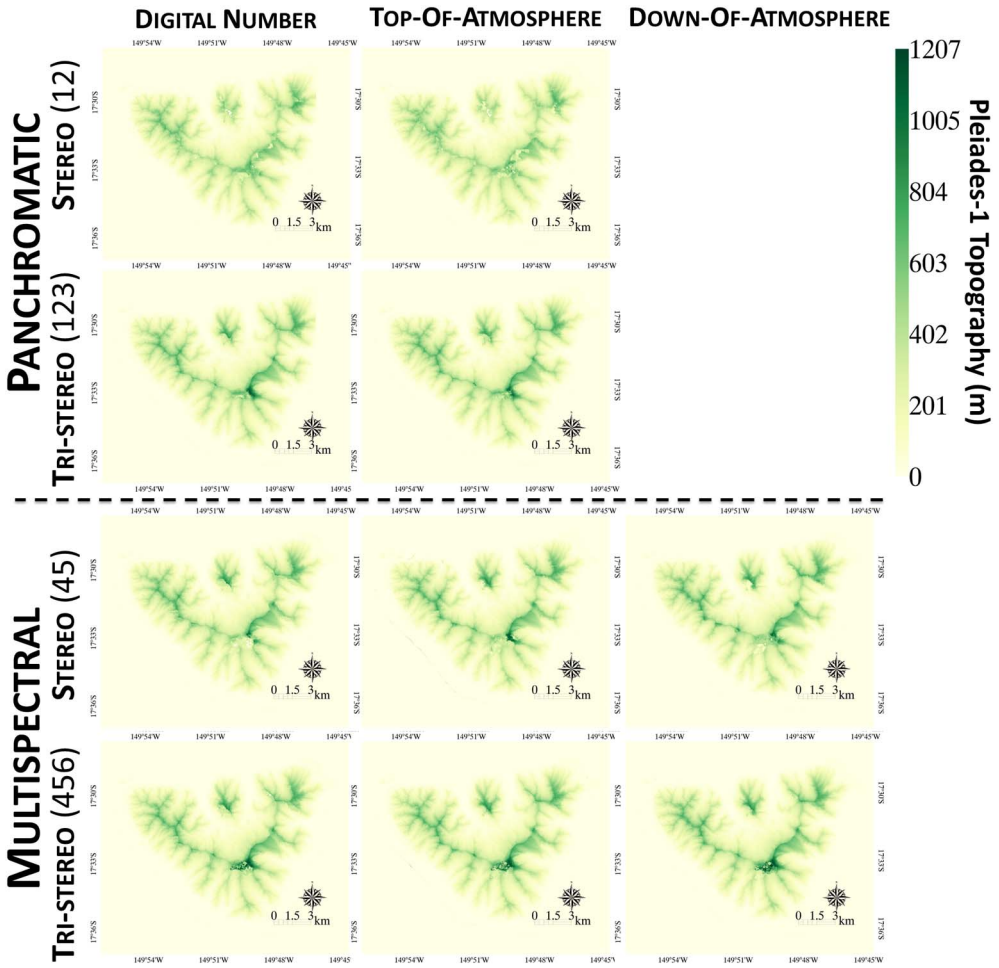

Fig. 6. Topography digital surface models (m) generated for three levels of radiometric corrections (digital number, top-of-atmosphere and down-of-atmosphere) and two photogrammetric modes (stereo and tri-stereo) as a function of Pleiades-1 spectral datasets (panchromatic and multispectral). The color ramp is based on the MSL. (For interpretation of the references to color in this figure legend, the reader is referred to the web version of this article.)

without radiometric correction (E_{RMSE} = 4.22 m and N_{RMSE} = 7.59 m). Since the radiometric correction counter-intuitively decreases the accuracy, we advocate to further investigate the adjacency effect associated with the atmospheric correction (here, MODTRAN4). Those accuracies are in agreement with a recent study testing the P-1 triplet: E_{RMSE} = 4.7 m and N_{RMSE} = 7.66 m (Perko et al., 2014). Another recent study (Topan et al., 2016), focused on P-1 stereo-based horizontal accuracies, showed better performances for easting ($E\mu_{RMSE}$ = 2.57 m) but lower ones for northing ($N\mu_{RMSE}$ = 8.02 m). The geometric correction applied in our study is purposefully based only on sensor orientation RPCs for the sake of repeatability in inaccessible remote areas. However, geolocation errors are strongly diminished (sub-pixel accuracy) when RPC-based imagery is referenced to GCPs (Perko et al., 2014; Gruen and Troyer, 2017), whose effect is augmented with tie points when the DSM is generated with ERDAS IMAGINE photogrammetry toolbox (Eisank et al., 2015; Gruen and Troyer, 2017). Adjusted P-1 triplet images thereafter produced DSM with horizontal accuracy 12 and 24 times better for easting and northing, respectively (E_{RMSE} = 0.38 m and N_{RMSE} = 0.31 m, Perko et al., 2014).

4.2. Drivers of the height accuracy

Relationships between P-1 and LiDAR topography showed positive intercepts for all datasets (Fig. 7). Those results indicate that P-1 topography reconstruction consistently overestimated actual topography. This result is contrary to Eisank et al. (2015), which was validated by a 3080–3170 m LiDAR range in Sulden (Italy). The height accuracy distinctly responded to the spatio-spectral mode, scene coverage and radiometry level. The highest accuracy was found with the panchromatic triplet corrected at the TOA level (RMSE = 7.40 m), which sensibly matched other studies' results (from 6.12 to 6.73 m in Poli et al., 2013, and from 4.07 to 6.4 m in Perko et al., 2014). Our slightly worse accuracy might be explained by the difference in validation elevation ranges (0–300 m range in Moorea versus 240–300 m in Trento, Italy, Poli et al., 2013 and Perko et al., 2014). The panchromatic spatio-spectral mode did not provide better results than multispectral mode (with initial coarser spatial resolution but with four spectral wavebands). The radiometric correction (from DN to TOA) exclusively benefited the panchromatic triplet and multispectral stereo datasets. Shifting from the computer DN to physical TOA values led to better height accuracy, what shows the importance of spectral reflectance that might facilitate the matching algorithm. The atmospheric correction (from TOA to DOA) did not conduct to better accuracy, what spurs to assess the adequacy of the atmospheric correction (here, MODTRAN4) with Pleiades-1 imagery, in the context of water-laden tropical air.

Given the relative high scores of multispectral datasets and the considerably faster computation time observed with those datasets compared to panchromatic ones, ratios of point density by computation time and topography DSM accuracy by computation time have been created (Fig. 11). Whereas four panchromatic datasets surpassed six multispectral datasets in point density per minute ratio, multispectral DN and TOA stereo outperformed the best panchromatic datasets in DSM accuracy per minute ratio.

In line with horizontal accuracy, the addition of GCPs is

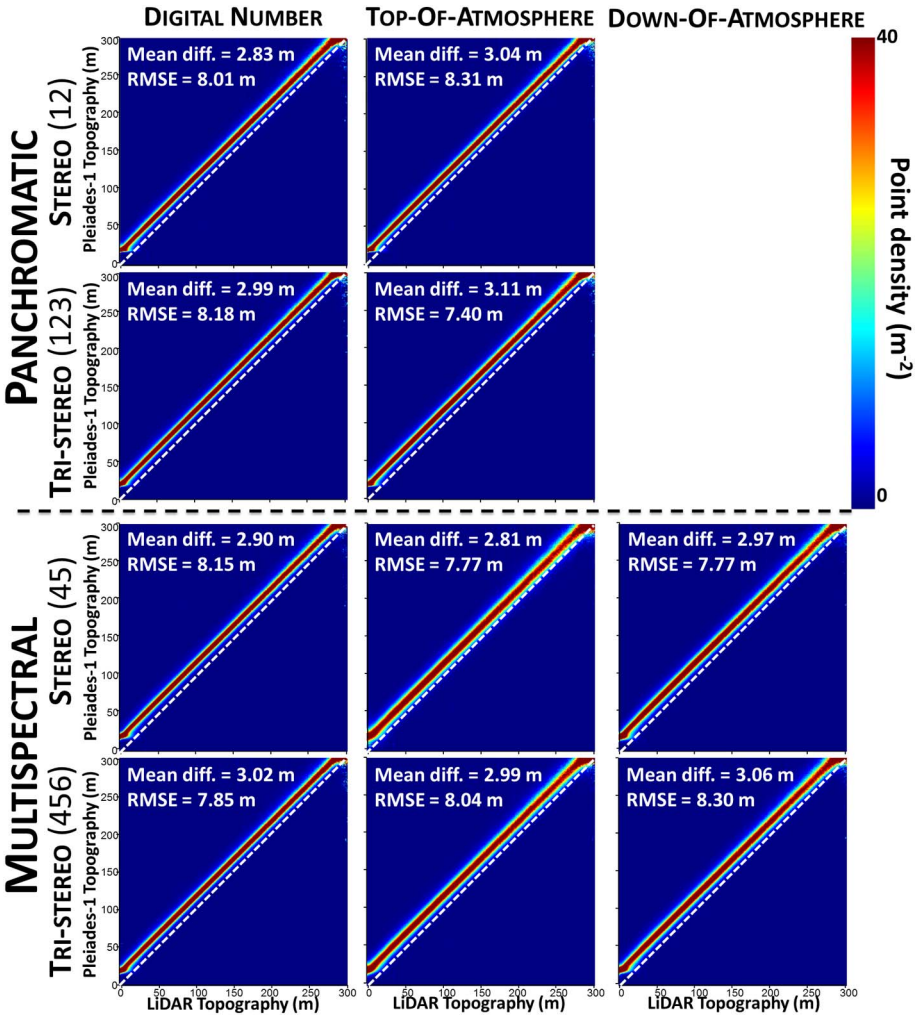

Fig. 7. Scatterplots (N = 1,511,273 points) between Pleiades-1 and LiDAR surface topography (m) generated for three levels of radiometric corrections (digital number, top-of-atmosphere and down-of-atmosphere) and two photogrammetric modes (stereo and tri-stereo) as a function of Pleiades-1 spectral datasets (panchromatic and multispectral).

recommended, wherever possible, to significant improve height accuracy, like in Trento test site, where 4.07–6.4 m range shifted to 1.11–3.35 m range (Perko et al., 2014). Another way topography accuracy improvement may arise from the enhancement of spatial resolution associated with the DEM used in preliminary steps of the point cloud generation. The 30-arcsecond GMTED, used in this study (ENVI source), could be replaced by finer global DEMs such as the freely available 1-arcsecond GDEM v2 (Tachikawa et al., 2011) or the commercial 12-m WorldDEM™ (Airbus).

4.3. Drivers of the depth accuracy

The radiometric correction had significant influence on the bathymetry DSM accuracy when retrieved from quasi-nadiral (mono) multispectral imagery. While DN's high score (level 0) dataset overtook TOA (level 1) one, it was topped by the DOA (level 2) one. Contrary to topography, bathymetry modelling at native multispectral spatial resolution requires spectral values to be corrected for atmosphere (see Collin and Hench, 2012 with WorldView-2 results). Our TOA

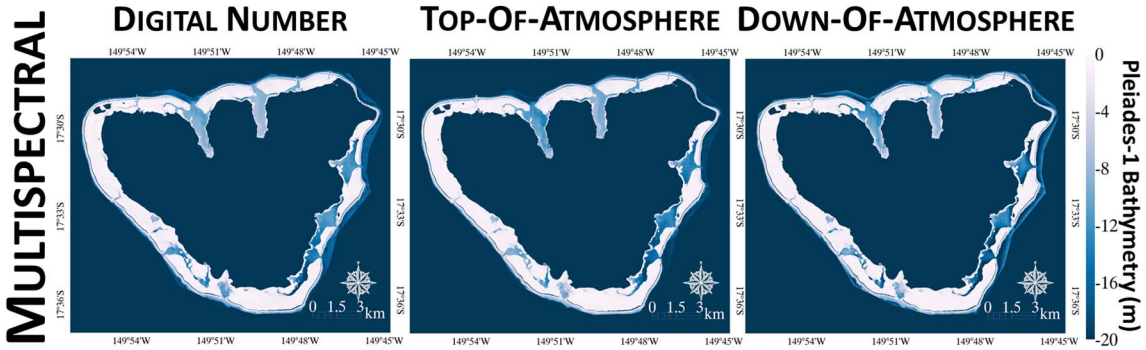

Fig. 8. Bathymetry digital surface models (m) generated for three levels of radiometric corrections (digital number, top-of-atmosphere and down-of-atmosphere) applied to quasi-nadiral Pleiades-1 multispectral dataset. The color ramp is based on the MSL. (For interpretation of the references to color in this figure legend, the reader is referred to the web version of this article.)

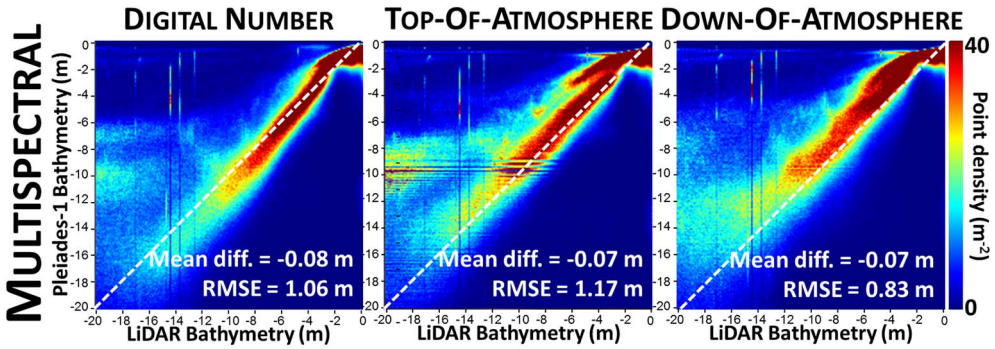

Fig. 9. Scatterplots (N = 2,417,704 points) between Pleiades-1 and LiDAR surface bathymetry (m) generated for three levels of radiometric corrections (digital number, top-of-atmosphere and down-of-atmosphere) applied to quasi-nadiral Pleiades-1 multispectral dataset.

performance (RMSE = 1.17 m) surpassed bathymetry retrieval using TOA P-1 spectral information (RMSE = 3.09 m, Collin and Hench, 2015). The latter study modeled Moorea bathymetry through 15,777 ground-truth soundings (200-kHz SoNAR) located in northern part of the lagoon. Moreover, our DOA performance (RMSE = 0.83 m) strongly outperformed DOA results of the latter study (RMSE = 4.65 m). This difference might be due to the extremely large number of LiDAR validation points evenly distributed over Moorea's various shallow habitats (see Fig. 2).

Despite our desire to extract topobathymetry without in situ

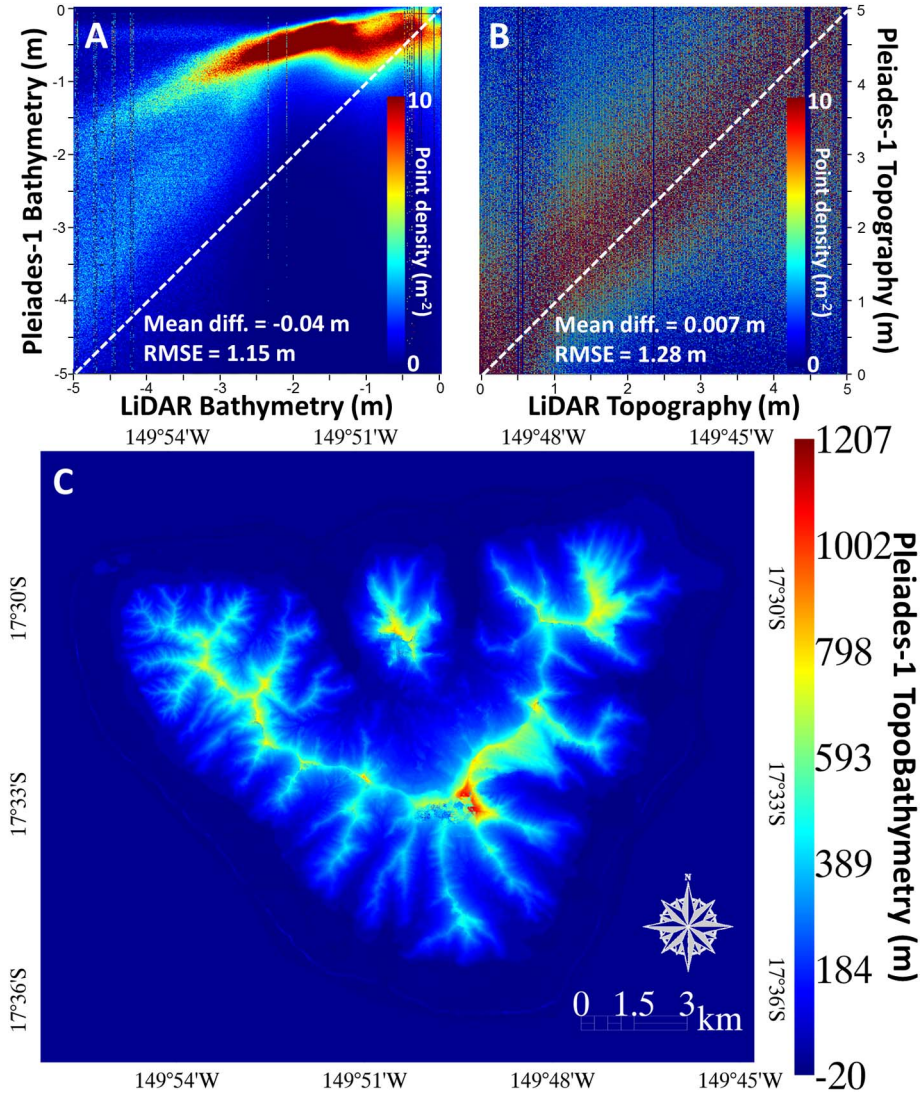

Fig. 10. Scatterplots between Pleiades-1 and LiDAR surface (A) −5-to-0-m bathymetry (N = 604,426), and (B) 0-to5-m topography (N = 25,188). (C) Topobathymetry digital surface model (DSM) of Moorea Island (ranging from −20 to 1207 m) based on the seam of the topography DSM derived from panchromatic tri-stereo top-of-atmosphere imagery and the bathymetry DSM derived from multispectral quasi-nadiral (mono) down-of-atmosphere imagery. The color ramp is based on the MSL. (For interpretation of the references to color in this figure legend, the reader is referred to the web version of this article.)

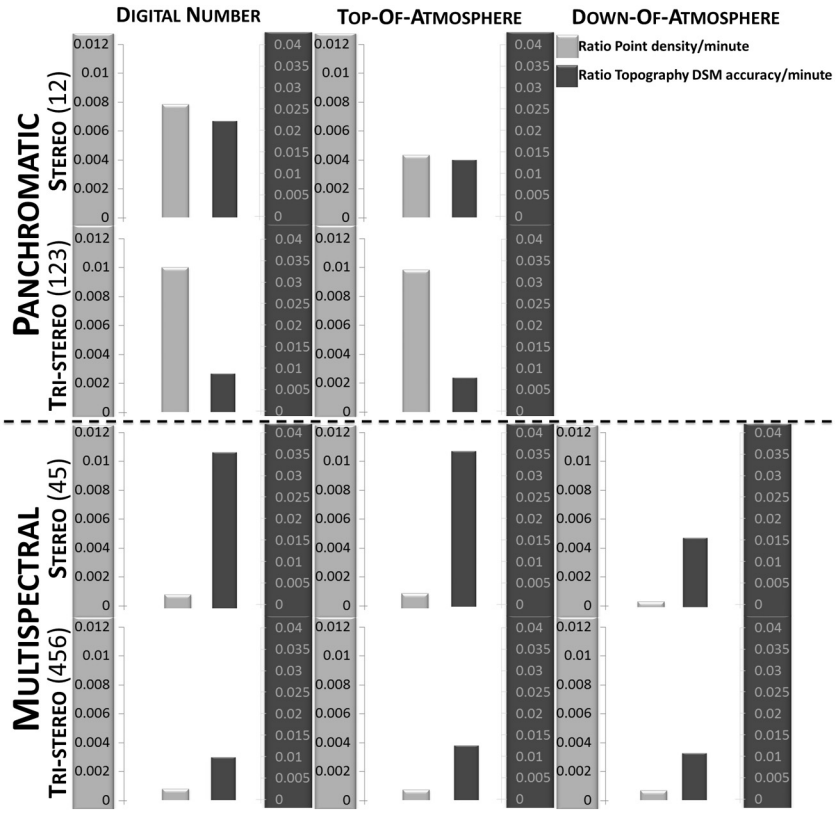

Fig. 11. Ratio of the point number per computation minute (light grey) and ratio of the topography DSM accuracy per computation minute generated for three levels of radiometric corrections (digital number, top-of-atmosphere and down-of-atmosphere) and two photogrammetric modes (stereo and tri-stereo) as a function of Pleiades-1 spectral datasets (panchromatic and multispectral).

samples, our bathymetry modelling, based on the ratio transform, necessitated calibration (here, 100 values from *SHOM* navigational chart data). In order to liberate from any ground-truth, we propose to constrain analytical tools (e.g. BOMBER, Giardino et al., 2012), estimating water quality and bottom properties from hyperspectral imagery, to multispectral P-1 imagery, since no calibration is required.

5. Conclusion

This research has shown that P-1 triplet imagery is a robust solution to model accurate topobathymetry across remote coasts with very few ground-truth provided that distinct workflows for topography (based on photogrammetry) and bathymetry (based on spectral transform) areas are implemented. The main findings can be summarized as follows:

1. Depending on the computation capacity (here, Core i7, with 32 Gb RAM) and research objectives, we advocate testing multispectral stereo datasets whose results are satisfactory before launching computationally intensive calculations with panchromatic tri-stereo datasets.
2. Horizontal accuracy was higher with tri-stereo (than stereo) either panchromatic (E_{RMSE} = 4.22 and N_{RMSE} = 7.59 m) or multispectral (E_{RMSE} = 5.06 and N_{RMSE} = 7.51 m) datasets but without radiometric correction.
3. Topography density of point clouds increased by three with tri-stereo either panchromatic (9.11 points·m^{-2}) or multispectral (0.23 points·m^{-2}) datasets but slightly decreased with radiometric correction.
4. Topography vertical accuracy increased with tri-stereo + TOA correction (RMSE = 7.40 m) for panchromatic and with stereo + TOA/DOA correction (RMSE = 7.77/7.77 m) as well as tri-stereo without radiometric correction (RMSE = 7.85 m) for multispectral datasets
5. Topography point density per minute ratio is maximized by panchromatic datasets (from 0.004 to 0.01), but DN and TOA multispectral datasets provide the best topography vertical accuracy per minute ratio (0.035)
6. Bathymetry vertical accuracy increased with atmospheric correction (DOA, RMSE = 0.83 m)

The DSM reconstruction of the coastal fringe based only a P-1 triplet imagery and some sparse bathymetric ground-truth enabled detailed and accurate modelling of the structural complexity of land and sea habitats in the coastal zone. Accuracy in mono-geometry bathymetry modelling overcame topography one, mostly due to a largest range in elevation, presence of the multi-storey vegetation and modelling based on pixel matching, impeding pixel-scale products. An exciting further step is to use multispectral data draped over the structure to classify socio-ecological patches, seamlessly. The integrated vision of the ridge to reefscape will help users and managers make sound ecosystem-based stewardship decisions in coastal spatial planning for food production (agriculture/forestry/fishery), water and soil management (geomorphology/hydrology), urbanism, and conservation (Davies et al., 2016).

Conflicts of interest

None.

Data availability

Satellite data are available publicly at http://observatoire.criobe.pf/wiki/tiki-index.php. Data can be accessed by completing and signing a form so that researchers agree to acknowledge SO CORAIL in any publications resulting from the use of the data. LiDAR data are partly publicly at http://data.shom.fr by selecting Master data, Coastal altimetry and *LiDAR Polynésie française* 2015, and partly property of the *Service de l'Urbanisme de la Polynésie Française*. To access these data, interested researcher may contact Pascal Correia-Baretto (tel.: 40 468 033).

Acknowledgments

Authors gratefully thank *SHOM* for LiDAR acquisition and validation, and the IDEA Consortium for sparking this collaborative research. This work was partly supported by French Polynesia Government for LiDAR acquisition, the ETH Zurich for satellite purchase and the National Science Foundation through the Moorea Coral Reef LTER (OCE-1236905 and 1637396) and Physical Oceanography (OCE-143133) programs. The paper has gained insights thanks to three anonymous reviewers' suggestions.

References

Becker, J.J., Sandwell, D.T., Smith, W.H.F., Braud, J., Binder, B., Depner, J., ... Ladner, R., 2009. Global bathymetry and elevation data at 30 arc seconds resolution: SRTM30_PLUS. Mar. Geod. 32 (4), 355–371.

Capaldo, P., Crespi, M., Fratarcangeli, F., Nascetti, A., Pieralice, F., 2012. DSM generation from high resolution imagery: applications with WorldView-1 and Geoeye-1. Italian Journal of Remote Sensing/Rivista Italiana di Telerilevamento 44 (1), 41–53.

Casella, E., Collin, A., Harris, D., Ferse, S., Bejarano, S., Parravicini, V., ... Rovere, A., 2016. Mapping coral reefs using consumer-grade drones and structure from motion photogrammetry techniques. Coral Reefs 36 (1), 269–275.

Collin, A., Hench, J.L., 2012. Towards deeper measurements of tropical reefscape structure using the WorldView-2 spaceborne sensor. Remote Sens. 4 (5), 1425–1447.

Collin, A., Hench, J.L., 2015. Extracting Shallow Bathymetry From Very High Resolution Satellite SPECTRAL bands and a Machine Learning Algorithm. 24 International Council of the Exploration of the Sea (ICES) CM.

Collin, A., Long, B., Archambault, P., 2012. Merging land-marine realms: spatial patterns of seamless coastal habitats using a multispectral LiDAR. Remote Sens. Environ. 123, 390–399.

Collin, A., Archambault, P., Planes, S., 2013. Bridging ridge-to-reef patches: seamless classification of the coast using very high resolution satellite. Remote Sens. 5 (7), 3583–3610.

Collin, A., Nadaoka, K., Nakamura, T., 2014. Mapping VHR water depth, seabed and land cover using Google Earth data. ISPRS Int. J. Geo-Information 3 (4), 1157–1179.

Collin, A., Etienne, S., Feunteun, E., 2017. VHR coastal bathymetry using WorldView-3: colour versus learner. Int. J. Remote Sens. 8 (11), 1072–1081.

Cressey, D., 2015. Tropical paradise inspires virtual ecology lab. Nature 517, 255–256.

Danielson, J.J., Gesch, D.B., 2011. Global Multi-resolution Terrain Elevation Data 2010 (GMTED2010) (No. 2011–1073). US Geological Survey.

Davies, N., Field, D., Gavaghan, D., Holbrook, S.J., Planes, S., Troyer, M., Bonsall, M., Claudet, J., Roderick, G., Schmitt, R.J., Zettler, L.A., Berteaux, V., Bossin, H.C., Cabasse, C., Collin, A., Deck, J., Dell, T., Dunne, J., Gates, R., Harfoot, M., Hench, J.L., Hopuare, M., Kirch, P., Kotoulas, G., Kosenkov, A., Kusenko, A., Leichter, J.J., Lenihan, H., Magoulas, A., Martinez, N., Meyer, C., Stoll, B., Swalla, B., Tartakovsky, D.M., Murphy, H.T., Turyshev, S., Valdvinos, F., Williams, R., Wood, S., 2016. Consortium I: simulating social-ecological systems: the island digital ecosystem avatars (IDEA) consortium. Gigascience 5, 14.

Eisank, C., Rieg, L., Klug, C., Kleindienst, H., Sailer, R., 2015. Semi-global matching of Pléiades tri-stereo imagery to generate detailed digital topography for high-alpine regions. GI_Forum 168–177.

Farr, T.G., Rosen, P.A., Caro, E., Crippen, R., Duren, R., Hensley, S., Kobrick, M., Paller, M., Rodriguez, E., Roth, L., Seal, D., Shaffer, S., Shimada, J., Umland, J., Werner, M., Oskin, M., Burbank, D., Alsdorf, S., 2007. The shuttle radar topography mission. Rev. Geophys. 45 (2).

Fonstad, M.A., Dietrich, J.T., Courville, B.C., Jensen, J.L., Carbonneau, P.E., 2013. Topographic structure from motion: a new development in photogrammetric measurement. Earth Surf. Process. Landf. 38 (4), 421–430.

Gehrke, S., Morin, K., Downey, M., Boehrer, N., Fuchs, T., 2010. Semi-global matching: an alternative to LIDAR for DSM generation. In: Proceedings of the Canadian Geomatics Conference and Symposium of Commission I. Vol. 2. pp. 1–6.

Gesch, D.B., Brock, J.C., Parrish, C.E., Rogers, J.N., Wright, C.W., 2016. Introduction: special issue on advances in topobathymetric mapping, models, and applications. J. Coast. Res. 76 (sp1), 1–3.

Giardino, C., Candiani, G., Bresciani, M., Lee, Z., Gagliano, S., Pepe, M., 2012. BOMBER: a tool for estimating water quality and bottom properties from remote sensing images. Comput. Geosci. 45, 313–318.

Gruen, A., Troyer, M., 2017. MooreaIDEA Land- and Seascape (on-line accessed on November 14, 2017).

Guenther, G.C., Brooks, M.W., LaRocque, P.E., 2000. New capabilities of the "SHOALS" airborne Lidar bathymeter. Remote Sens. Environ. 73 (2), 247–255.

Hayakawa, Y.S., Oguchi, T., Lin, Z., 2008. Comparison of new and existing global digital elevation models: ASTER G-DEM and SRTM-3. Geophys. Res. Lett. 35 (17).

Hayes, M.P., Gough, P.T., 2009. Synthetic aperture sonar: a review of current status. IEEE J. Ocean. Eng. 34 (3), 207–224.

Johnstone, E., Raymond, J., Olsen, M.J., Driscoll, N., 2016. Morphological expressions of coastal cliff erosion processes in San Diego County. J. Coast. Res. 76 (sp1), 174–184.

Kress, M.E., Benimoff, A.I., Fritz, W.J., Thatcher, C.A., Blanton, B.O., Dzedzits, E., 2016. Modeling and simulation of storm surge on Staten Island to understand inundation mitigation strategies. J. Coast. Res. 76 (sp1), 149–161.

Olson, C.J., Becker, J.J., Sandwell, D.T., 2014. A new global bathymetry map at 15 arc-second resolution for resolving seafloor fabric: SRTM15_PLUS. In: AGU Fall Meeting Abstracts.

Pe'eri, S., Madore, B., Nyberg, J., Snyder, L., Parrish, C., Smith, S., 2016. Identifying bathymetric differences over Alaska's North Slope using a satellite-derived bathymetry multi-temporal approach. J. Coast. Res. 76 (sp1), 56–63.

Perko, R., Raggam, H., Gutjahr, K., Schardt, M., 2014. Assessment of the mapping potential of Pléiades stereo and triplet data. In: ISPRS Annals of the Photogrammetry, Remote Sensing and Spatial Information Sciences. 2(3). pp. 103–109.

Poli, D., Remondino, F., Angiuli, E., Agugiaro, G., 2013. Evaluation of Pleiades-1a triplet on Trento testfield. Int. Arch. Photogramm. Remote. Sens. Spat. Inf. Sci. 40, 287–292.

Riegler, G., Hennig, S.D., Weber, M., 2015. WorldDEM-a novel global foundation layer. Int. Arch. Photogramm. Remote. Sens. Spat. Inf. Sci. 40 (3), 183.

Sandwell, D.T., Smith, W.H., 1997. Marine gravity anomaly from Geosat and ERS 1 satellite altimetry. J. Geophys. Res. Solid Earth 102 (B5), 10039–10054.

Service Hydrographique et Océanographique de la Marine (SHOM), 2016. Readme-Produit-maritime-SAU-MOO2015_V20160630. (on-line accessed on November 8, 2017).

Service Hydrographique et Océanographique de la Marine (SHOM), 2017. Références altimétriques maritimes. In: Cotes du zéro hydrographique et niveaux caractéristiques de la marée. SHOM, France, pp. 99–100.

Stumpf, R.P., Holderied, K., Sinclair, M., 2003. Determination of water depth with high-resolution satellite imagery over variable bottom types. Limnol. Oceanogr. 48 (1part2), 547–556.

Tachikawa, T., Hato, M., Kaku, M., Iwasaki, A., 2011. Characteristics of ASTER GDEM version 2. In: Geoscience and Remote sensing symposium (IGARSS), pp. 3657–3660.

Topan, H., Cam, A., Özendi, M., Oruç, M., Jacobsen, K., Taşkanat, T., 2016. Pléiades project: assessment of georeferencing accuracy, image quality, pansharpening performance and DSM/DTM quality. Int. Arch. Photogramm. Remote. Sens. Spat. Inf. Sci.-ISPRS Arch. 41, 503–510.

Toutin, T., 2004a. DTM generation from Ikonos in-track stereo images using a 3D physical model. Photogramm. Eng. Remote. Sens. 70 (6), 695–702.

Toutin, T., 2004b. DSM generation and evaluation from QuickBird stereo imagery with 3D physical modelling. Int. J. Remote Sens. 25 (22), 5181–5192.